

# Enhancing Spatial Understanding in Image Generation via Reward Modeling

Zhenyu Tang<sup>1,2\*</sup> Chaoran Feng<sup>1\*</sup> Yufan Deng<sup>1,2</sup> Jie Wu<sup>2</sup> Xiaojie Li<sup>2</sup>  
 Rui Wang<sup>2</sup> Yunpeng Chen<sup>2</sup> Daquan Zhou<sup>1</sup>  
<sup>1</sup>Peking University <sup>2</sup>ByteDance Seed

## Abstract

Recent progress in text-to-image generation has greatly advanced visual fidelity and creativity, but it has also imposed higher demands on prompt complexity—particularly in encoding intricate spatial relationships. In such cases, achieving satisfactory results often requires multiple sampling attempts. To address this challenge, we introduce a novel method that strengthens the spatial understanding of current image generation models. We first construct the **SpatialReward-Dataset** with over 80k preference pairs. Building on this dataset, we build **SpatialScore**, a reward model designed to evaluate the accuracy of spatial relationships in text-to-image generation, achieving performance that even surpasses leading proprietary models on spatial evaluation. We further demonstrate that this reward model effectively enables online reinforcement learning for the complex spatial generation. Extensive experiments across multiple benchmarks show that our specialized reward model yields significant and consistent gains in spatial understanding for image generation. The visual demo is available at the [project page](#).

## 1. Introduction

Recent advances in generative models [12, 22, 24, 27, 33, 42, 44, 57, 58] have transformed visual content creation, enabling the synthesis of high-fidelity and diverse images [6, 8, 18, 35, 39, 51]. Following the success of online reinforcement learning (RL) [41] in large language models [10, 31], recent studies [11, 21, 25, 46, 48, 54, 61] have explored applying GRPO-style reinforcement learning to diffusion models, leading to significant performance gains.

However, with increasing prompt complexity, text-to-image models often struggle to accurately depict scenes that involve complex spatial relationships among multiple objects. This motivates us to explore how to enhance the spatial understanding of image generation models. Reinforcement learning emerges as a promising direction to address

\*Equal Contribution.

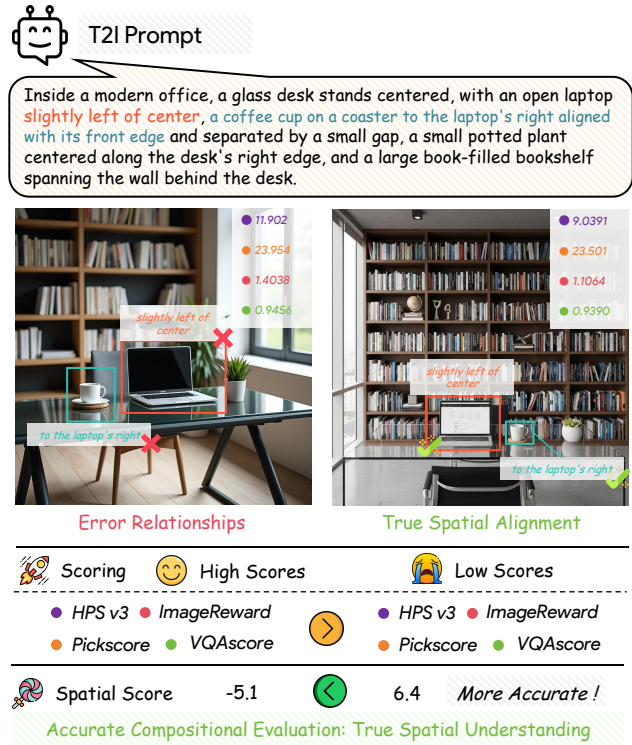


Figure 1. **Failure of Reward Models on Spatial Understanding.** Existing reward models [17, 23, 29, 53] often assign higher reward values to spatially incorrect images than to spatially correct ones, thereby exposing their limited spatial reasoning capabilities.

this challenge. However, despite its theoretical potential, applying online RL to improve spatial understanding remains difficult—primarily due to the lack of a reliable and effective reward model.

A straightforward approach is to adopt existing image reward models. As shown in Figure 1, human-preference reward models [17, 29, 49, 52, 53] which incorporate text-image alignment as one of the evaluation factors, fail to accurately evaluate complex spatial relationships, and reward models [15, 23] designed for text-image alignment, which rely on VQA-style evaluations, exhibit the same limitation. The second option is to leverage the latest proprietary APIs of visual language models (VLM) [7, 32]. How-

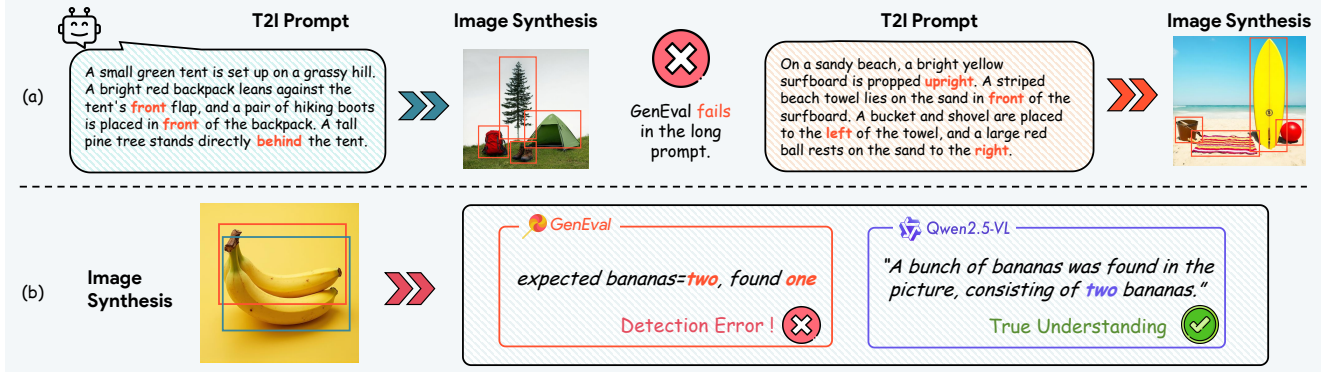


Figure 2. Limitations of GenEval [9] as the reward model. (a) GenEval-based RL training fails to generalize to long prompts involving complex spatial relationships across multiple objects. (b) The rule-based GenEval rewards, which rely on object detectors, often produce incorrect evaluations under visual challenges like occlusion, while modern VLMs can accurately infer the correct response.

ever, their high cost makes them impractical for online RL, which requires frequent reward queries. The third alternative is to utilize open-source VLMs. However, our experiments show that even advanced models such as Qwen2.5-VL-72B [3] suffer from substantial hallucinations and fail to provide reliable and accurate rewards, possibly because they are not optimized for complex reasoning on spatial relationships across multiple objects.

Recent works such as Flow-GRPO [25] have also explored compositional generation on the rule-based GenEval benchmark [9], which computes rewards with an object detector and a color classifier. However, GenEval includes only simple prompts of the form "a photo of A <relative position> B." In Figure 2, we observe that training on GenEval fails to generalize to longer prompts with multiple spatial relationships, and its reward computation is highly sensitive to visual factors such as occlusion, leading to inaccurate rewards.

In this work, we argue that enhancing spatial understanding in image generation through online RL relies on constructing a reliable and accurate reward model. We first introduce SPATIALREWARD-DATASET, which contains 80K adversarial preference pairs spanning a wide range of real-world scenarios. Each preference pair is collected through an adversarial setup consisting of one image that accurately aligns with complex spatial relationships described in the prompt and one perturbed image that violates part of these relationships. To ensure data quality and accuracy, all pairs are carefully reviewed and filtered by human experts.

Building on this dataset, we further train SPATIALSCORE, a powerful reward model designed to evaluate the accuracy of spatial relationships in image generation. Our results show that SpatialScore even surpasses several leading proprietary models, which exhibit hallucinations when reasoning about complex spatial relationships among multiple objects.

We further employ SpatialScore as the reward model for online RL. To improve training efficiency, we propose a top- $k$  filtering strategy that maintains a balanced sampling ratio between high-reward and low-reward candidates. The results on multiple benchmarks show that our approach effectively leverages feedback from SpatialScore, leading to substantial performance improvements over its base model.

Our contributions are summarized as follows:

- We introduce SPATIALREWARD-DATASET with over 80K adversarial preference pairs, carefully curated by humans to ensure data quality.
- We develop SPATIALSCORE, a strong reward model for evaluating spatial relationship accuracy in image generation, which surpasses several leading proprietary models.
- We employ SpatialScore as the reward model for online RL with a top- $k$  filtering strategy. Extensive experiments show substantial improvements in spatial understanding for image generation over the base model.

## 2. Related Works

### 2.1. Reward Model in T2I models

Reward models are crucial for the success of reinforcement learning (RL) by providing the high-quality signals required for policy optimization. HPSv2 [52], Pickscore [17], Aesthetic score [5], and the works [20, 23, 59] fine-tune CLIP-based model with human preference data, and HPSv3 [29] and UnifiedReward [49] employ Vision-Language Models (VLMs) as the backbone for reward generation in the text-to-image task. However, while these models excel at assessing aesthetic quality and overall text-image alignment, they often lack the fine-grained capacity to comprehend and evaluate complex spatial relationships across multiple objects. This limitation can lead to generations that are semantically plausible but compositionally incorrect, which motivates our development of a specialized reward model

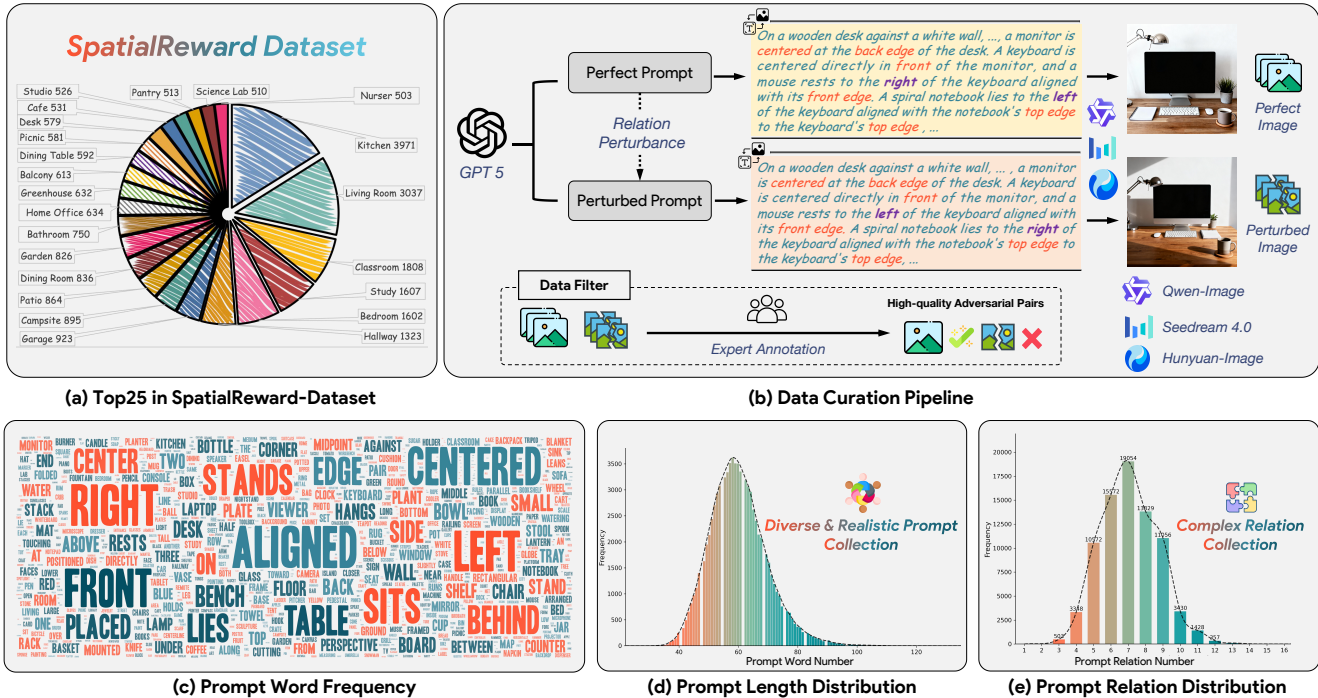


Figure 3. Overview of our SpatialReward-Dataset.

that focuses on spatial understanding.

## 2.2. Reinforcement Learning in Image Generation

Reinforcement learning has been effectively applied in diffusion models to improve generation quality. Proximal Policy Optimization (PPO) [40] and Direct Preference Optimization (DPO) [36] originally developed for large language models, have been successfully adapted to diffusion-based generation [16, 20, 37, 53, 62], improving task alignment and controllability. Building upon this, to pursue a more stable and efficient optimization process, Flow-GRPO [25], Dance-GRPO [54] and others [11, 21, 46, 48, 60] have integrated the flow model with Group Relative Policy Optimization (GRPO) [10]. They transform deterministic ordinary differential equation (ODE) sampling into stochastic differential equation (SDE) [2, 43] to facilitate policy exploration. Our work differs by introducing a spatially-aware reward model tailored for spatial understanding in image generation, providing reliable feedbacks.

## 3. Dataset

Building on VideoAlign [26], which demonstrates that preference learning outperforms pointwise score regression for reward training, we introduce the carefully curated adversarial SPATIALREWARD-DATASET as the foundation for subsequent reward training.

As illustrated in Figure 3, we construct the SPATIALREWARD DATASET comprising 80K adversarial pairs. In Fig-

ure 3(a), we illustrate the diverse real-world scenarios used in our data construction. To minimize the influence of other attributes, such as aesthetic differences across image generation models, we generate each preference pair using a single image generation model with distinct prompts. Specifically, we first use GPT-5 to create a set of initial prompts featuring complex spatial relationships among multiple objects. We then employ GPT-5 to perturb these clean prompts by modifying one or more spatial relations (e.g., moving an object from left to right, swapping relative positions of objects) while keeping the remaining spatial relationships unchanged. Under this setup, the images generated from the original, unperturbed prompts serve as the *perfect* images, whereas those generated from the perturbed prompts act as the *perturbed* images.

For data construction, we employ several state-of-the-art image generation models Qwen-Image [51] and HunyuanImage-2.1 [45] and seedream4.0 [8], which demonstrate strong text-image alignment capabilities, thereby reducing extensive data filtering. Each data pair is manually reviewed and validated by human annotators to filter out cases where the *perfect* image fails to fully align with the complex spatial constraints described in the prompt, ensuring high data quality for reward training. More details of the construction of the SpatialReward-Dataset are provided in the *Appendix*. As shown in Figure 3(d), our carefully curated dataset contains significantly longer prompts compared to GenEval [9], indicating higher

scene complexity. Moreover, in Figure 3(e), these prompts involve multiple spatial relationships among objects, leading to a greater degree of spatial complexity and compositional diversity than the simple and template-based constructions presented in the Geneval benchmark.

## 4. Method: SpatialScore

### 4.1. Architecture

Recently, Visual Language Models (VLMs) have achieved remarkable progress and been widely applied to various vision–language tasks such as grounding [30, 34, 56] and segmentation [19, 38, 55]. Their success largely stems from training on massive web-scale datasets and learning highly generalizable representations.

Building upon the strong representational power of VLMs as feature extractors, we adopt a VLM as the backbone of our reward model. Specifically, we use Qwen2.5-VL-7B [3] as the backbone  $H_\phi$  to extract features from both images and text, while replacing the original language modeling head with a new linear reward head  $R_\phi$  that projects the features to predict the reward value. Our reward model is trained on preference pairs consisting of a preferred image  $y_w$  as the “winner” and a less preferred image  $y_l$  as the “loser”, given an instruction prompt  $c$ . The reward score  $s$  for a generated image is computed as:

$$s = R_\phi(H_\phi(c, y)). \quad (1)$$

For each preference pair, the scores  $s_w$  and  $s_l$  are obtained by feeding the preferred image  $y_w$  and the less preferred image  $y_l$  into the model, respectively.

### 4.2. Reward training

To build our SPATIALSCORE reward model, we fine-tune Qwen2.5-VL-7B using the LoRA [13] to preserve the inherent knowledge priors of the model. In our SPATIALREWARD-DATASET setup, each training example is represented as a triplet  $(c, y_w, y_l)$ , where  $y_w$  and  $y_l$  correspond to the perfect image and the perturbed image generated from the perturbed prompt, respectively.

Inspired by HPSv3 [29], which models the reward score as a probability distribution for more robust ranking instead of directly outputting a deterministic value, we adopt a Gaussian distribution  $s \sim \mathcal{N}(\mu, \sigma^2)$  to model the final reward score, where  $\mu$  and  $\sigma$  denote the mean and standard deviation, respectively. Specifically, within the VLM instruction setup, we insert a special token `<reward>` at the end of the full prompt, allowing it to attend to both the image and text representations. The final-layer embedding of this special token is then mapped to  $\mu$  and  $\sigma$  through the reward head  $R_\phi$ , implemented as a multilayer perceptron (MLP). In this way, we model the output score by sampling from this one-dimensional Gaussian distribution.

Finally, the training process involves two independent forward passes of the reward model for each triplet sample  $(c, y_w, y_l)$  to obtain the reward scores of  $y_w$  and  $y_l$ . The reward model is optimized following the Bradley-Terry model [4] by minimizing the negative log-likelihood of the ground-truth preference using a binary cross-entropy loss:

$$P(y_w \succ y_l | c) = \sigma\left(R_\phi(H_\phi(y_w, c)) - R_\phi(H_\phi(y_l, c))\right), \quad (2)$$

$$\mathcal{L}_{\text{Reward}}(\theta) = \mathbb{E}_{c, y_w, y_l}[-\log P(y_w \succ y_l | c)]. \quad (3)$$

Here,  $\sigma$  denotes the sigmoid function, which constrains the output to a probability value within the interval  $[0, 1]$ , and  $\theta$  represents the trainable parameters of the reward model. Through the optimization of  $\mathcal{L}_{\text{Reward}}$ , our reward model learns to assign higher scores to the preferred images over less-preferred ones. Once trained, SpatialScore serves as the reward model for online reinforcement learning, further enhancing spatial understanding in image generation.

## 5. SpatialScore in Image Generation

With the high-fidelity and specialized reward model SPATIALSCORE, we then leverage it as a direct reward signal for online reinforcement learning fine-tuning in order to validate the effectiveness of our reward model.

We choose FLUX.1-dev [18] as our base model for image generation due to its advanced performance and strong support for handling long text inputs, which aligns well with the complex prompt setting of our SPATIALREWARD-DATASET. Moreover, FLUX.1-dev has not undergone the post-training stage, making it an ideal choice to fairly evaluate the potential gains introduced by our reward model. As shown in the Figure 4, we employ the GRPO algorithm from FlowGRPO [25] and leverage our reward model to provide reliable feedback for optimizing the base generation model for spatial understanding.

Specifically, as an online RL algorithm, GRPO [41] requires diverse samples within a group to optimize the policy and evaluate the reward uplift direction. However, flow matching inherently employs a deterministic ODE for sampling, whereas RL relies on stochasticity for policy exploration. Following Flow-GRPO [25], we convert the deterministic ODE into an equivalent SDE that shares the same marginal distribution. The resulting SDE can be discretized using the Euler–Maruyama scheme as follows:

$$x_{t+\Delta t} = x_t + \left[ v_\theta(x_t, t) + \frac{\sigma_t^2}{2t} (x_t + (1-t)v_\theta(x_t, t)) \right] \Delta t + \sigma_t \sqrt{\Delta t} \epsilon \quad (4)$$

where  $\epsilon \sim \mathcal{N}(0, I)$  denotes standard Gaussian noise,  $\sigma_t$  represents the injected noise level, and  $v_\theta(x_t, t)$  denotes the estimated velocity field.

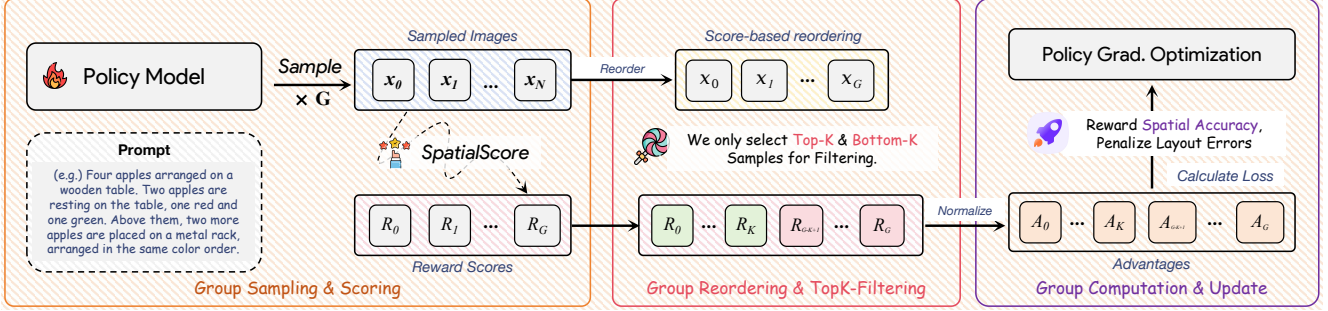


Figure 4. **GRPO training pipeline for enhancing spatial understanding.** We first sample a group of images from the policy model and use our specialized SpatialScore to rate their spatial accuracy. After ranking based on these scores, we select the top- $k$  most accurate and bottom- $k$  least accurate examples and convert these scores into advantage signals. The policy model is updated via policy gradient optimization to directly reward correct spatial layouts and penalize errors, thereby enhancing the base model’s spatial understanding.

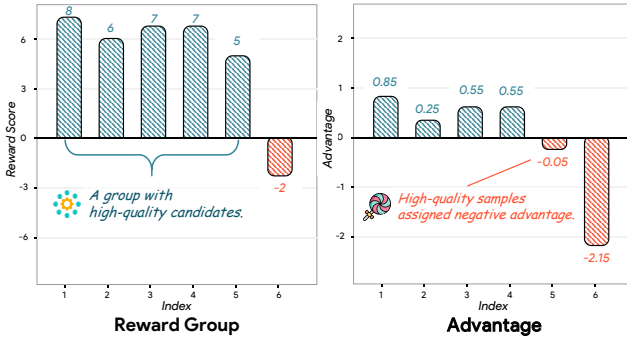


Figure 5. **Advantage bias.** For easy prompts with many high-reward samples, some high-quality samples often obtain negative advantages due to the high group mean.

For each prompt  $c$  sampled from our SPATIALREWARD-DATASET, the base model as the policy  $\pi_\theta$  generates a group of  $G$  images  $\{x_0^i\}_{i=1}^G$  through SDE sampling. Our reward model SPATIALSCORE then evaluates each generated image  $x_0^i$  conditioned on  $c$  and assigns a reward score  $R(x_0^i, c)$ . Within each group, the advantage  $A^i$  of the  $i$ -th image is computed by normalizing its reward with respect to the group mean and standard deviation:

$$A^i = \frac{R(x_0^i, c) - \text{mean}(\{R(x_0^j, c)\}_{j=1}^G)}{\text{std}(\{R(x_0^j, c)\}_{j=1}^G)}. \quad (5)$$

Based on the preliminary findings in Flow-GRPO [25], a sufficiently large group size is essential to ensure diverse sampling and stabilize training. However, in our practical experiments, as online RL training progresses, prompts of varying difficulty may cause biased advantage estimation. Specifically, easy prompts tend to accumulate a large number of successful samples with high reward scores within a group, while difficult prompts often produce samples with generally low rewards. As illustrated in Figure 5, for an easy prompt, the group-wise normalization may yield a high mean value, which in turn assigns negative advantages to some high-quality samples, producing optimization gradi-

ents that deviate from the intended reward-improvement direction. Conversely, hard prompts also yield advantage bias.

To mitigate advantage biases across prompts of varying difficulty, we propose a top- $k$  filtering strategy. Specifically, for a sampled group of  $G$  images  $\{x_0^i\}_{i=1}^G$  generated by the policy  $\pi_\theta$ , we rank them based on the reward scores estimated by our reward model, obtaining a sorted sequence  $\{\hat{x}_0^i\}_{i=1}^G$ . To balance the reward distribution within the group and further mitigate advantage bias, we select both the top- $k$  and bottom- $k$  samples to form an index subset, i.e.,  $S = \{1, 2, \dots, k, G - k + 1, \dots, G\}$ , which is then used to compute the group mean and standard deviation. During policy updates, only these selected samples in this subset  $S$  are utilized for training.

The GRPO algorithm then optimizes the policy by minimizing the following objective:

$$\mathcal{L}_{\text{GRPO}}(\theta) = \frac{1}{|S|} \sum_{i \in S} \frac{1}{T} \sum_{t=0}^{T-1} \min(r_t^i(\theta) A_t^i, \text{clip}(r_t^i(\theta), 1 - \epsilon, 1 + \epsilon) A_t^i). \quad (6)$$

where  $r_t^i(\theta) = \frac{p_\theta(\hat{x}_{t-1}^i | \hat{x}_t^i, c)}{p_{\theta_{\text{old}}}(\hat{x}_{t-1}^i | \hat{x}_t^i, c)}$ . An additional KL-divergence penalty term  $D_{\text{KL}}(\pi_\theta \| \pi_{\text{ref}})$  is introduced to regularize the policy  $\pi_\theta$  and prevent excessive deviation from the reference policy  $\pi_{\text{ref}}$ . This ensures that the generation model is directly optimized toward improved spatial understanding, driven by feedback from our reward model.

Our GRPO optimization reduces the number of function evaluations (NFE) required for updating the policy  $\pi_\theta$  compared to optimizing over all samples within each group. Following the empirical results of Flow-GRPO [25], which indicate that directly reducing the sampling group size might lead to training collapse for GRPO, we maintain a consistent group size with Flow-GRPO to ensure sufficient sample diversity during sampling.

Table 1. Pairwise-accuracy comparisons on the reward evaluation benchmark. “1 Pert.” and “2–3 Pert.” denote subsets with one or two–three spatial perturbations applied to the perfect prompts when constructing the perturbed prompts.

Setting	Image Reward Models					Qwen2.5-VL Series			Proprietary Models		SpatialScore	
	Image Reward	PickScore	HPSv2.1	VQAScore	Unified Reward	HPSv3	7B	32B	72B	GPT-5		Gemini-2.5 pro
1 Pert.	0.439	0.461	0.433	0.567	0.583	0.606	0.572	0.644	0.711	0.855	0.933	<b>0.939</b>
2–3 Pert.	0.513	0.551	0.491	0.638	0.627	0.697	0.632	0.724	0.816	0.924	0.968	<b>0.978</b>
Overall	0.479	0.509	0.463	0.603	0.605	0.652	0.602	0.685	0.764	0.890	0.951	<b>0.958</b>

Table 2. Detailed comparisons on SpatialScore, DPG-Bench, TIIF-Bench (short/long), and UnigenBench++ (short/long). \* denotes training with Geneval as the reward model. BR, AR, and RR denote basic relation, attribute+relation, and relation+reasoning. Lay-2D/3D refer to layout-2D/3D. Unibench denotes UniGenBench++.

Method	SpatialScore	DPG-bench	TIIF-bench-short			TIIF-bench-long			Unibench(short)		Unibench(long)	
		Relation-Spatial	BR	AR	RR	BR	AR	RR	Lay-2D	Lay-3D	Lay-2D	Lay-3D
Flux.1-dev [18]	2.18	0.871	0.769	0.608	0.584	0.758	0.677	0.645	0.766	0.667	0.819	0.742
Flow-GRPO* [25]	3.01	0.742	0.851	0.652	0.621	0.577	0.510	0.482	0.726	0.635	0.445	0.405
Ours	<b>7.81</b>	<b>0.932</b>	<b>0.875</b>	<b>0.700</b>	<b>0.647</b>	<b>0.845</b>	<b>0.715</b>	<b>0.675</b>	<b>0.875</b>	<b>0.773</b>	<b>0.891</b>	<b>0.801</b>

## 6. Experiments

### 6.1. Experimental Settings

**Implementation Details.** For reward model training, our SPATIALSCORE is built by fine-tuning Qwen2.5-VL-7B [3] with LoRA [13] on our curated SPATIALREWARD-DATASET, which contains 80K preference pairs. The training completes within one day on eight NVIDIA H20 GPUs, using a learning rate of  $2 \times 10^{-6}$  and a gradient accumulation batch size of 32. For RL training, we apply the trained SPATIALSCORE as the reward model to fine-tune the base model Flux.1-dev [18] which supports long-text prompts for complex scenes in an online RL setup. Following Flow-GRPO [25], we adopt LoRA-based fine-tuning for GRPO training, with a LoRA rank of 32, a learning rate of  $3 \times 10^{-4}$ , an importance clipping range of  $1 \times 10^{-4}$ , a group size of 24, and a KL-penalty coefficient of 0.01. The online RL training is conducted on 32 NVIDIA H20 GPUs.

**Evaluation Benchmarks for SpatialScore.** For reward model evaluation, we construct a high-quality and diverse benchmark consisting of 365 preference pairs. Following a process similar to SPATIALREWARD-DATASET, we generate *perturbed* prompts by perturbing the original *perfect* prompts. Each prompt pair is then generated to images using Qwen-Image [51], HunyuanImage-2.1 [45] and Seedream-4.0 [8], followed by meticulous human review and verification to ensure annotation reliability. We evaluate a wide range of leading models on this benchmark using overall preference accuracy as the metric. The evaluation includes proprietary models such as GPT-5 [32] and Gemini-2.5 [7], advanced open-source VLMs from

the Qwen2.5-VL [3] series from 7B to 72B, and several existing image reward models, including PickScore [17], ImageReward [53], UnifiedReward [49], and the HPS series [29, 52]. For UnifiedReward, we employ the Qwen2.5-VL-based models with superior performance.

**Evaluation Benchmarks in image generation.** For evaluating the spatial understanding of image generation models, we first employ our proposed reward model SPATIALSCORE to assess in-domain performance in spatial reasoning. Beyond in-domain evaluation, we further adopt several out-of-domain benchmarks designed to measure text–image alignment, from which we select the spatial-aware sub-dimensions to specifically evaluate spatial understanding in image generation. In particular, we utilize DPG-Bench [14], which focuses on complex text-to-image alignment; TIIF-Bench [50], an extension of T2I-Compbench++ [47] to long prompts, evaluated by GPT-4o [1]; and the recently released UniGenBench++ [47], which is assessed by Gemini-2.5 Pro [7].

### 6.2. Reward Model Performance

Building upon our carefully curated SPATIALREWARD-DATASET, we propose a state-of-the-art specialized reward model SPATIALSCORE for evaluating spatial understanding: the accuracy of complex spatial relationships among multiple objects. As shown in Table 1, we compare the accuracy of preference prediction against a broad set of baselines, including human-preference reward models, reward models tailored for text–image alignment, advanced open-source vision language models (VLMs), and the proprietary models. To analyze robustness across difficulty levels, we

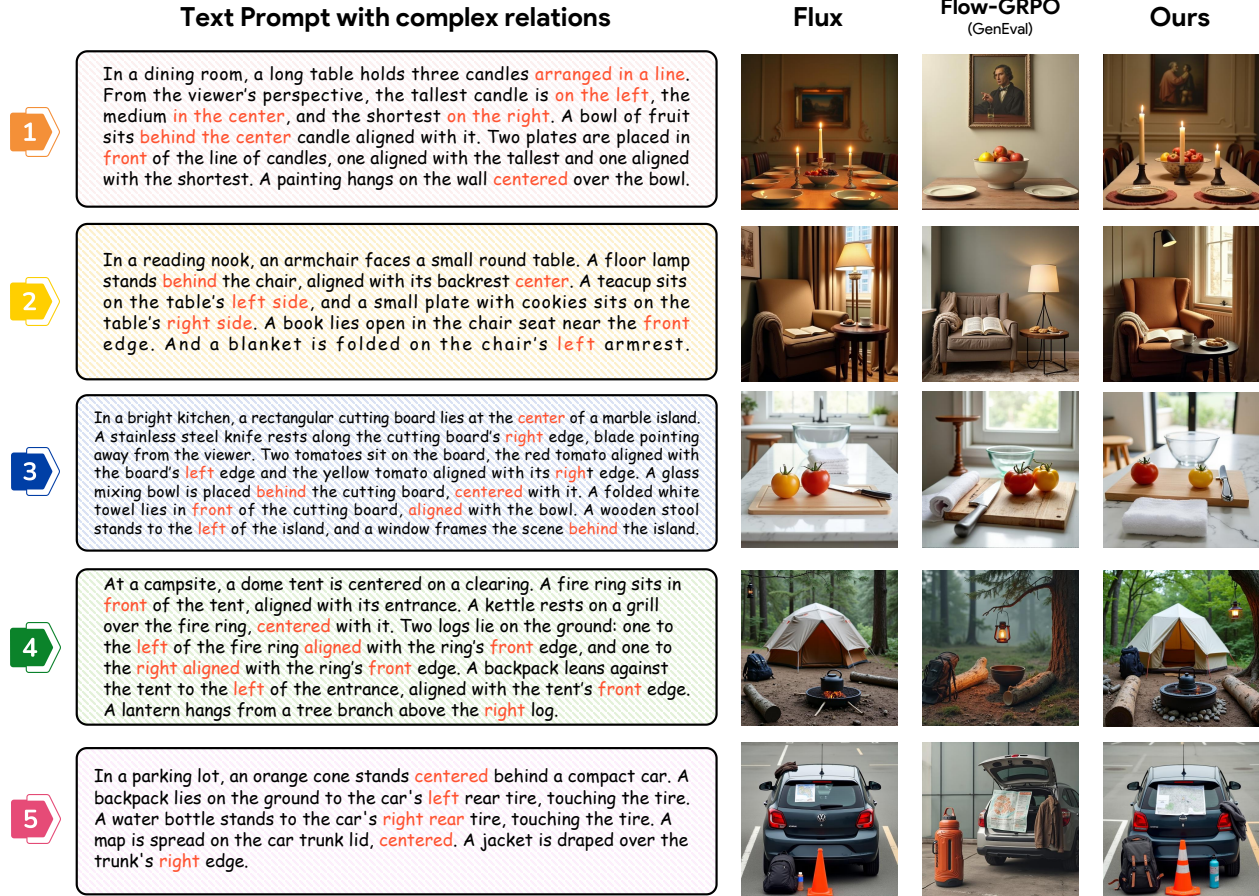


Figure 6. Qualitative comparison on prompts with complex spatial relationships across multiple objects.

split our built benchmark by the number of spatial perturbations applied to the *perfect* prompt to construct the *perturbed* prompt: a 1-perturbation subset and a 2-3 perturbation subset, while keeping all other spatial relations unchanged during data construction.

As shown in Table 1, proprietary models achieve consistently higher preference-prediction accuracy than both open-source vision language models (VLMs) and existing image-reward models on our benchmark. Leading proprietary models such as GPT-5 [32] and Gemini-2.5 Pro [7] constitute the top tier, attaining the accuracies from 0.89 to 0.95, which shows their strong zero-shot spatial understanding for image generation. However, their high per-query cost makes them impractical for the frequent evaluations required by online RL. By contrast, existing image-reward models, which consider text-image alignment, exhibit limited ability to assess multi-object spatial reasoning, attaining limited pairwise accuracies. Open-source VLMs also exhibit clear limitations. Although the Qwen2.5-VL series shows a scaling trend in spatial understanding from 7B to 72B parameters, the 72B variant reaches only 0.76 pairwise accuracy, well below proprietary models, and the 7B and 32B models perform even worse. These results in-

dicates that current advanced open-source VLMs are not yet reliable providers of rewards for complex spatial reasoning.

In contrast, our SPATIALSCORE with 7B parameters achieves state-of-the-art results on the reward benchmark, reaching a pairwise accuracy of 95.77%. It surpasses strong proprietary models, including GPT-5 and Gemini-2.5 Pro, on spatial understanding across multiple objects. These results indicate that our specialized reward model can provide a reliable and stable reward signal for online RL.

### 6.3. Applying SpatialScore for Online RL

**Quantitative results.** Guided by our specialized reward model SPATIALSCORE, we perform online RL training using Flux.1-dev as the base model. As shown in Table 2, we compare with the original base model and a variant from Flow-GRPO trained on GenEval for compositional image generation across multiple benchmarks. On the in-domain SPATIALSCORE evaluation, our approach improves the score from 2.18 to 7.81, demonstrating the effectiveness of reward-guided training. To further assess spatial understanding, we evaluate several text-image alignment benchmarks and select their spatial-aware subdimensions. Our RL training yields consistent gains on both short- and long-

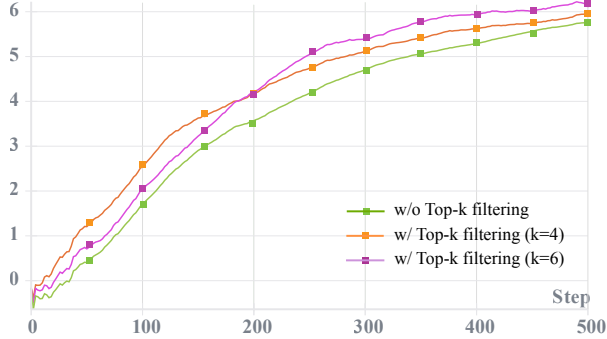


Figure 7. Reward training curves for ablations on top- $k$  filtering

Table 3. Full-dimensional comparison on DPG-Bench. The best Flux variants are in **bold**, and \* denotes training with GenEval.

Method	Global	Entity	Attribute	Relation	Other	Overall
GPT-Image-1	88.89	88.94	89.84	92.63	90.96	85.15
Flux.1-dev	84.70	87.29	89.29	89.44	89.46	82.91
Flow-GRPO*	69.20	72.37	69.23	73.26	69.72	57.02
Ours	<b>87.65</b>	<b>90.56</b>	<b>91.20</b>	<b>91.58</b>	<b>86.43</b>	<b>85.03</b>

prompt settings. In contrast, the model trained with Flow-GRPO on the rule-based GenEval shows some improvement on short prompts but degrades markedly on long-prompt settings, indicating limited generalization to long prompts with complex multi-object spatial relationships.

**Qualitative results.** As shown in Figure 6, we present qualitative comparisons against the original Flux.1-dev model and the variant trained with Flow-GRPO on the rule-based GenEval benchmark. Our RL-trained model using the specialized SPATIALSCORE exhibits improved spatial understanding, producing images that more faithfully reflect the complex spatial relationships across multiple objects described in the prompts. In contrast, the Flux.1-dev variant trained with Flow-GRPO on GenEval demonstrates limited ability to generalize to complex spatial compositions and even loses part of the base model’s long-prompt following capability. As shown in Figure 6, this includes missing key objects such as the candles in example (1) and the tent in example (4). Moreover, due to the reliance on rule-based rewards from object detectors, the GenEval-guided model frequently generates visually implausible artifacts, such as floating maps or jackets, as seen in example (5).

**Out-of-domain evaluation.** We further conduct a full-spectrum evaluation on DPG-Bench [14], a benchmark designed to assess text–image alignment. As shown in Table 3, our method yields consistent and substantial improvements over the original Flux.1-dev model across all five major dimensions of DPG-Bench, with gains observed beyond the spatial subdimension. Notably, the overall performance of our RL-enhanced model approaches that of the proprietary GPT-Image-1. In contrast, the Flux variant trained with Flow-GRPO on GenEval exhibits clear degradation.

## 6.4. Ablation Study

**Ablations on reward model size.** To assess the generalizability of our approach, we train SPATIALSCORE with varying backbone sizes. On our reward evaluation benchmark, SPATIALSCORE improves the accuracy of pairwise preference prediction from 89.1% to 95.8% when scaling the backbone from Qwen2.5-VL-3B to Qwen2.5-VL-7B. More additional results are provided in the Appendix.

Table 4. Ablations on top- $k$  filtering. NFE per prompt for each training step is reported under a denoising step count of 6.

Setting	SpatialScore	DPG-bench	Unigenbench++ (long)		NFE
		Rel-Spatial	Layout-2D	Layout-3D	
w/o top- $k$	7.73	0.919	<b>0.891</b>	0.793	24*6
w/ top- $k$ ( $k=4$ )	7.71	0.916	0.882	0.796	<b>8*6</b>
w/ top- $k$ ( $k=6$ )	<b>7.81</b>	<b>0.932</b>	0.887	<b>0.801</b>	12*6

**Ablations on top- $k$  filtering.** In online RL training, prompts of varying difficulty can lead to highly imbalanced reward distributions within a group. In particular, easy prompts often produce many high-reward samples, which obtain high group mean and consequently assign negative advantages to some high-quality samples. To mitigate this issue, we apply a top- $k$  filtering strategy that selects the top- $k$  and bottom- $k$  samples within the group to construct a balanced subset and reduce advantage bias. As shown in Figure 7, adding top- $k$  filtering accelerates training compared to the baseline GRPO setup without filtering. When  $k = 4$ , the training exhibits faster early-stage improvement but slows down in later stages due to insufficient sample diversity. In contrast,  $k = 6$  maintains a better tradeoff between sampling balance and diversity, and we adopt  $k = 6$  as the default configuration in all experiments. As shown in Table 4, we observe that using  $k = 6$  achieves comparable or even superior performance with fewer the number of function evaluations (NFE) in the policy update stage. With a sampling group size of 24 and denoising steps of 6, only 2\*6\*6 NFEs per prompt when  $k = 6$  at each step for training stage, whereas the original RL needs 24\*6 NFEs.

## 7. Conclusion

In this work, we address the challenge of improving spatial understanding in image generation through online RL. To this end, we first introduce the SPATIALREWARD-DATASET, an 80K-pair preference dataset curated with rigorous human verification. Building on this dataset, we develop SPATIALSCORE, a specialized reward model that provides reliable signals and achieves evaluation accuracy surpassing even proprietary models. Leveraging this high-fidelity reward model and GRPO framework with top- $k$  filtering, we obtain substantial and consistent improvements in spatial reasoning across multiple benchmarks over the base model.

## References

- [1] Gpt-4o. <https://openai.com/index/hello-gpt-4o/>. 6, 2
- [2] Michael S Albergo, Nicholas M Boffi, and Eric Vandenberg. Stochastic interpolants: A unifying framework for flows and diffusions. *arXiv preprint arXiv:2303.08797*, 2023. 3
- [3] Shuai Bai, Keqin Chen, Xuejing Liu, Jialin Wang, Wenbin Ge, Sibao Song, Kai Dang, Peng Wang, Shijie Wang, Jun Tang, et al. Qwen2. 5-vl technical report. *arXiv preprint arXiv:2502.13923*, 2025. 2, 4, 6, 1
- [4] Ralph Allan Bradley and Milton E Terry. Rank analysis of incomplete block designs: I. the method of paired comparisons. *Biometrika*, 39(3/4):324–345, 1952. 4
- [5] Laura Jannes Burger. Laion: Image data, ai, and dispossession. Master’s thesis, 2023. 2
- [6] Siyu Cao, Hangting Chen, Peng Chen, Yiji Cheng, Yutao Cui, Xincheng Deng, Ying Dong, Kipper Gong, Tianpeng Gu, Xiuse Gu, et al. Hunyuanimage 3.0 technical report. *arXiv preprint arXiv:2509.23951*, 2025. 1
- [7] Gheorghe Comanici, Eric Bieber, Mike Schaekermann, Ice Pasupat, Noveen Sachdeva, Inderjit Dhillon, Marcel Blisstein, Ori Ram, Dan Zhang, Evan Rosen, et al. Gemini 2.5: Pushing the frontier with advanced reasoning, multimodality, long context, and next generation agentic capabilities. *arXiv preprint arXiv:2507.06261*, 2025. 1, 6, 7, 2, 4
- [8] Yu Gao, Lixue Gong, Qiushan Guo, Xiaoxia Hou, Zhichao Lai, Fanshi Li, Liang Li, Xiaochen Lian, Chao Liao, Liyang Liu, et al. Seedream 3.0 technical report. *arXiv preprint arXiv:2504.11346*, 2025. 1, 3, 6, 2
- [9] Dhruva Ghosh, Hannaneh Hajishirzi, and Ludwig Schmidt. Geneval: An object-focused framework for evaluating text-to-image alignment. *Advances in Neural Information Processing Systems*, 36:52132–52152, 2023. 2, 3
- [10] Daya Guo, Dejian Yang, Haowei Zhang, Junxiao Song, Ruoyu Zhang, Runxin Xu, Qihao Zhu, Shirong Ma, Peiyi Wang, Xiao Bi, et al. Deepseek-r1: Incentivizing reasoning capability in llms via reinforcement learning. *arXiv preprint arXiv:2501.12948*, 2025. 1, 3
- [11] Xiaoxuan He, Siming Fu, Yuke Zhao, Wanli Li, Jian Yang, Dacheng Yin, Fengyun Rao, and Bo Zhang. Tempflow-grpo: When timing matters for grpo in flow models. *arXiv preprint arXiv:2508.04324*, 2025. 1, 3
- [12] Jonathan Ho, Ajay Jain, and Pieter Abbeel. Denoising diffusion probabilistic models. *Advances in neural information processing systems*, 33:6840–6851, 2020. 1
- [13] Edward J Hu, Yelong Shen, Phillip Wallis, Zeyuan Allen-Zhu, Yuanzhi Li, Shean Wang, Lu Wang, Weizhu Chen, et al. Lora: Low-rank adaptation of large language models. *ICLR*, 1(2):3, 2022. 4, 6, 1
- [14] Xiwei Hu, Rui Wang, Yixiao Fang, Bin Fu, Pei Cheng, and Gang Yu. Ella: Equip diffusion models with llm for enhanced semantic alignment. *arXiv preprint arXiv:2403.05135*, 2024. 6, 8, 2
- [15] Yushi Hu, Benlin Liu, Jungo Kasai, Yizhong Wang, Mari Ostendorf, Ranjay Krishna, and Noah A Smith. Tifa: Accurate and interpretable text-to-image faithfulness evaluation with question answering. In *Proceedings of the IEEE/CVF International Conference on Computer Vision*, pages 20406–20417, 2023. 1
- [16] Dongzhi Jiang, Ziyu Guo, Renrui Zhang, Zhuofan Zong, Hao Li, Le Zhuo, Shilin Yan, Pheng-Ann Heng, and Hongsheng Li. T2i-r1: Reinforcing image generation with collaborative semantic-level and token-level cot. *arXiv preprint arXiv:2505.00703*, 2025. 3
- [17] Yuval Kirstain, Adam Polyak, Uriel Singer, Shabbuland Matiana, Joe Penna, and Omer Levy. Pick-a-pic: An open dataset of user preferences for text-to-image generation. *Advances in neural information processing systems*, 36:36652–36663, 2023. 1, 2, 6
- [18] Black Forest Labs. Flux. <https://github.com/black-forest-labs/flux>, 2024. 1, 4, 6, 5
- [19] Xin Lai, Zhuotao Tian, Yukang Chen, Yanwei Li, Yuhui Yuan, Shu Liu, and Jiaya Jia. Lisa: Reasoning segmentation via large language model. In *Proceedings of the IEEE/CVF Conference on Computer Vision and Pattern Recognition*, pages 9579–9589, 2024. 4
- [20] Jialuo Li, Wenhao Chai, Xingyu Fu, Haiyang Xu, and Saining Xie. Science-t2i: Addressing scientific illusions in image synthesis. In *Proceedings of the Computer Vision and Pattern Recognition Conference*, pages 2734–2744, 2025. 2, 3
- [21] Junzhe Li, Yutao Cui, Tao Huang, Yinping Ma, Chun Fan, Miles Yang, and Zhao Zhong. Mixgrpo: Unlocking flow-based grpo efficiency with mixed ode-sde. *arXiv preprint arXiv:2507.21802*, 2025. 1, 3
- [22] Bin Lin, Yunyang Ge, Xinhua Cheng, Zongjian Li, Bin Zhu, Shaodong Wang, Xianyi He, Yang Ye, Shenghai Yuan, Lihuan Chen, et al. Open-sora plan: Open-source large video generation model. *arXiv preprint arXiv:2412.00131*, 2024. 1
- [23] Zhiqiu Lin, Deepak Pathak, Baiqi Li, Jiayao Li, Xide Xia, Graham Neubig, Pengchuan Zhang, and Deva Ramanan. Evaluating text-to-visual generation with image-to-text generation. In *European Conference on Computer Vision*, pages 366–384. Springer, 2024. 1, 2
- [24] Yaron Lipman, Ricky TQ Chen, Heli Ben-Hamu, Maximilian Nickel, and Matt Le. Flow matching for generative modeling. *arXiv preprint arXiv:2210.02747*, 2022. 1
- [25] Jie Liu, Gongye Liu, Jiajun Liang, Yangguang Li, Jiaheng Liu, Xintao Wang, Pengfei Wan, Di Zhang, and Wanli Ouyang. Flow-grpo: Training flow matching models via online rl. *arXiv preprint arXiv:2505.05470*, 2025. 1, 2, 3, 4, 5, 6
- [26] Jie Liu, Gongye Liu, Jiajun Liang, Ziyang Yuan, Xiaokun Liu, Mingwu Zheng, Xiele Wu, Qiulin Wang, Wenyu Qin, Menghan Xia, et al. Improving video generation with human feedback. *arXiv preprint arXiv:2501.13918*, 2025. 3
- [27] Xingchao Liu, Chengyue Gong, and Qiang Liu. Flow straight and fast: Learning to generate and transfer data with rectified flow. *arXiv preprint arXiv:2209.03003*, 2022. 1
- [28] Cheng Lu, Yuhao Zhou, Fan Bao, Jianfei Chen, Chongxuan Li, and Jun Zhu. Dpm-solver: A fast ode solver for diffusion probabilistic model sampling in around 10 steps. *Advances in neural information processing systems*, 35:5775–5787, 2022. 5

- [29] Yuhang Ma, Xiaoshi Wu, Keqiang Sun, and Hongsheng Li. Hpsv3: Towards wide-spectrum human preference score. In *Proceedings of the IEEE/CVF International Conference on Computer Vision*, pages 15086–15095, 2025. 1, 2, 4, 6
- [30] Shehan Munasinghe, Hanan Gani, Wenqi Zhu, Jiale Cao, Eric Xing, Fahad Shahbaz Khan, and Salman Khan. Videoglam: A large multimodal model for pixel-level visual grounding in videos. In *Proceedings of the Computer Vision and Pattern Recognition Conference*, pages 19036–19046, 2025. 4
- [31] OpenAI. Image generation API, 2025. Accessed: 2025-10-30. 1
- [32] OpenAI. Gpt-5 is here. <https://openai.com/gpt-5/>, 2025. Accessed: 2025-09-18. 1, 6, 7, 2
- [33] William Peebles and Saining Xie. Scalable diffusion models with transformers. In *Proceedings of the IEEE/CVF international conference on computer vision*, pages 4195–4205, 2023. 1
- [34] Zhiliang Peng, Wenhui Wang, Li Dong, Yaru Hao, Shaohan Huang, Shuming Ma, and Furu Wei. Kosmos-2: Grounding multimodal large language models to the world. *arXiv preprint arXiv:2306.14824*, 2023. 4
- [35] Dustin Podell, Zion English, Kyle Lacey, Andreas Blattmann, Tim Dockhorn, Jonas Müller, Joe Penna, and Robin Rombach. Sdxl: Improving latent diffusion models for high-resolution image synthesis. *arXiv preprint arXiv:2307.01952*, 2023. 1
- [36] Rafael Rafailov, Archit Sharma, Eric Mitchell, Christopher D Manning, Stefano Ermon, and Chelsea Finn. Direct preference optimization: Your language model is secretly a reward model. *Advances in neural information processing systems*, 36:53728–53741, 2023. 3
- [37] Allen Z Ren, Justin Lidard, Lars L Ankile, Anthony Simeonov, Pulkit Agrawal, Anirudha Majumdar, Benjamin Burchfiel, Hongkai Dai, and Max Simchowitz. Diffusion policy optimization. *arXiv preprint arXiv:2409.00588*, 2024. 3
- [38] Zhongwei Ren, Zhicheng Huang, Yunchao Wei, Yao Zhao, Dongmei Fu, Jiashi Feng, and Xiaojie Jin. Pixellm: Pixel reasoning with large multimodal model. In *Proceedings of the IEEE/CVF Conference on Computer Vision and Pattern Recognition*, pages 26374–26383, 2024. 4
- [39] Robin Rombach, Andreas Blattmann, Dominik Lorenz, Patrick Esser, and Björn Ommer. High-resolution image synthesis with latent diffusion models. In *Proceedings of the IEEE/CVF conference on computer vision and pattern recognition*, pages 10684–10695, 2022. 1
- [40] John Schulman, Filip Wolski, Prafulla Dhariwal, Alec Radford, and Oleg Klimov. Proximal policy optimization algorithms. *arXiv preprint arXiv:1707.06347*, 2017. 3
- [41] Zhihong Shao, Peiyi Wang, Qihao Zhu, Runxin Xu, Junxiao Song, Xiao Bi, Haowei Zhang, Mingchuan Zhang, YK Li, Yang Wu, et al. Deepseekmath: Pushing the limits of mathematical reasoning in open language models. *arXiv preprint arXiv:2402.03300*, 2024. 1, 4
- [42] Yang Song, Jascha Sohl-Dickstein, Diederik P Kingma, Abhishek Kumar, Stefano Ermon, and Ben Poole. Score-based generative modeling through stochastic differential equations. *arXiv preprint arXiv:2011.13456*, 2020. 1
- [43] Yang Song, Jascha Sohl-Dickstein, Diederik P Kingma, Abhishek Kumar, Stefano Ermon, and Ben Poole. Score-based generative modeling through stochastic differential equations. *arXiv preprint arXiv:2011.13456*, 2020. 3
- [44] Zhenyu Tang, Junwu Zhang, Xinhua Cheng, Wangbo Yu, Chaoran Feng, Yatian Pang, Bin Lin, and Li Yuan. Cycle3d: High-quality and consistent image-to-3d generation via generation-reconstruction cycle. In *Proceedings of the AAAI Conference on Artificial Intelligence*, pages 7320–7328, 2025. 1
- [45] Tencent Hunyuan Team. Hunyuanimage 2.1: An efficient diffusion model for high-resolution (2k) text-to-image generation. <https://github.com/Tencent-Hunyuan/HunyuanImage-2.1>, 2025. 3, 6, 2
- [46] Jing Wang, Jiajun Liang, Jie Liu, Henglin Liu, Gongye Liu, Jun Zheng, Wanyuan Pang, Ao Ma, Zhenyu Xie, Xintao Wang, Meng Wang, Pengfei Wan, and Xiaodan Liang. Grpoguard: Mitigating implicit over-optimization in flow matching via regulated clipping, 2025. 1, 3
- [47] Yibin Wang, Zhimin Li, Yuhang Zang, Jiazi Bu, Yujie Zhou, Yi Xin, Junjun He, Chunyu Wang, Qinglin Lu, Cheng Jin, et al. Unigenbench++: A unified semantic evaluation benchmark for text-to-image generation. *arXiv preprint arXiv:2510.18701*, 2025. 6, 2
- [48] Yibin Wang, Zhimin Li, Yuhang Zang, Yujie Zhou, Jiazi Bu, Chunyu Wang, Qinglin Lu, Cheng Jin, and Jiaqi Wang. Pref-grpo: Pairwise preference reward-based grpo for stable text-to-image reinforcement learning. *arXiv preprint arXiv:2508.20751*, 2025. 1, 3
- [49] Yibin Wang, Yuhang Zang, Hao Li, Cheng Jin, and Jiaqi Wang. Unified reward model for multimodal understanding and generation. *arXiv preprint arXiv:2503.05236*, 2025. 1, 2, 6
- [50] Xinyu Wei, Jinrui Zhang, Zeqing Wang, Hongyang Wei, Zhen Guo, and Lei Zhang. Tiif-bench: How does your t2i model follow your instructions? *arXiv preprint arXiv:2506.02161*, 2025. 6, 2
- [51] Chenfei Wu, Jiahao Li, Jingren Zhou, Junyang Lin, Kaiyuan Gao, Kun Yan, Sheng-ming Yin, Shuai Bai, Xiao Xu, Yilei Chen, et al. Qwen-image technical report. *arXiv preprint arXiv:2508.02324*, 2025. 1, 3, 6, 2, 4, 5
- [52] Xiaoshi Wu, Yiming Hao, Keqiang Sun, Yixiong Chen, Feng Zhu, Rui Zhao, and Hongsheng Li. Human preference score v2: A solid benchmark for evaluating human preferences of text-to-image synthesis. *arXiv preprint arXiv:2306.09341*, 2023. 1, 2, 6
- [53] Jiazheng Xu, Xiao Liu, Yuchen Wu, Yuxuan Tong, Qinkai Li, Ming Ding, Jie Tang, and Yuxiao Dong. Imagereward: Learning and evaluating human preferences for text-to-image generation. *Advances in Neural Information Processing Systems*, 36:15903–15935, 2023. 1, 3, 6
- [54] Zeyue Xue, Jie Wu, Yu Gao, Fangyuan Kong, Lingting Zhu, Mengzhao Chen, Zhiheng Liu, Wei Liu, Qiushan Guo, Weilin Huang, et al. Dancegrpo: Unleashing grpo on visual generation. *arXiv preprint arXiv:2505.07818*, 2025. 1, 3

- [55] Senqiao Yang, Tianyuan Qu, Xin Lai, Zhuotao Tian, Bohao Peng, Shu Liu, and Jiaya Jia. Lisa++: An improved baseline for reasoning segmentation with large language model. *arXiv preprint arXiv:2312.17240*, 2023. 4
- [56] Hao Zhang, Hongyang Li, Feng Li, Tianhe Ren, Xueyan Zou, Shilong Liu, Shijia Huang, Jianfeng Gao, Leizhang, Chunyuan Li, et al. Llava-grounding: Grounded visual chat with large multimodal models. In *European Conference on Computer Vision*, pages 19–35. Springer, 2024. 4
- [57] Junwu Zhang, Zhenyu Tang, Yatian Pang, Xinhua Cheng, Peng Jin, Yida Wei, Xing Zhou, Munan Ning, and Li Yuan. Repaint123: Fast and high-quality one image to 3d generation with progressive controllable repainting. In *European Conference on Computer Vision*, pages 303–320. Springer, 2024. 1
- [58] Kaiwen Zhang, Zhenyu Tang, Xiaotao Hu, Xingang Pan, Xiaoyang Guo, Yuan Liu, Jingwei Huang, Li Yuan, Qian Zhang, Xiao-Xiao Long, et al. Epona: Autoregressive diffusion world model for autonomous driving. In *Proceedings of the IEEE/CVF International Conference on Computer Vision*, pages 27220–27230, 2025. 1
- [59] Sixian Zhang, Bohan Wang, Junqiang Wu, Yan Li, Tingting Gao, Di Zhang, and Zhongyuan Wang. Learning multi-dimensional human preference for text-to-image generation. In *Proceedings of the IEEE/CVF Conference on Computer Vision and Pattern Recognition*, pages 8018–8027, 2024. 2
- [60] Yujie Zhou, Pengyang Ling, Jiazi Bu, Yibin Wang, Yuhang Zang, Jiaqi Wang, Li Niu, and Guangtao Zhai. G2rpo: Granular grpo for precise reward in flow models. *arXiv preprint arXiv:2510.01982*, 2025. 3
- [61] Yujie Zhou, Pengyang Ling, Jiazi Bu, Yibin Wang, Yuhang Zang, Jiaqi Wang, Li Niu, and Guangtao Zhai. G2rpo: Granular grpo for precise reward in flow models. *arXiv preprint arXiv:2510.01982*, 2025. 1
- [62] Huaisheng Zhu, Teng Xiao, and Vasant G Honavar. Dspo: Direct score preference optimization for diffusion model alignment. In *The Thirteenth International Conference on Learning Representations*, 2025. 3

# Enhancing Spatial Understanding in Image Generation via Reward Modeling

## Supplementary Material

### Contents

<b>8. Experimental Details</b>	<b>1</b>
8.1. Reward Model Training	1
8.2. Reward Model Evaluation	1
8.3. Applying SpatialScore for Online RL	1
8.4. Evaluations for Image Generation	1
<b>9. Dataset Construction</b>	<b>2</b>
9.1. Preference Pair Construction	2
9.2. Human Verifications	2
<b>10 Additional Experiment Results</b>	<b>4</b>
10.1 Applying SpatialScore to Qwen-Image	4
10.2 Evaluations on Geneval Benchmark	4
10.3 Ablations on Model Size	4
10.4 Understanding of Spatial Issues in T2I models	5
10.5 More Clarifications on NFE	5
10.6 More Visual Demos	5
<b>11 Limitations and Future Works</b>	<b>5</b>

## 8. Experimental Details

### 8.1. Reward Model Training

Our reward model SPATIALSCORE is constructed by fine-tuning Qwen2.5-VL-7B [3] with LoRA [13] on our curated SPATIALREWARD-DATASET, which consists of 80k preference pairs covering a wide range of real-world scenarios. During training, we insert a special token `<reward>` into the instruction to attend to both visual and textual features. The complete instruction template is shown in the textbox 8 on the top of the next page. The final-layer embedding of this special token is projected by the reward head  $R_\phi$  into the mean  $\mu$  and standard deviation  $\sigma$  of a Gaussian distribution, from which the final reward score is obtained through sampling. To enhance training stability, we sample 1000 times from the Gaussian distribution of both the preferred image  $y_w$  and the perturbed image  $y_l$  when computing  $\mathcal{L}_{\text{Reward}}$ , and use the average of these 1000 score pairs to compute the final loss. Training completes within one day on 8 NVIDIA H20 GPUs, using a learning rate of  $2 \times 10^{-6}$ , a batch size of 16, and gradient accumulation steps of 2.

### 8.2. Reward Model Evaluation

Similar to the construction of the SPATIALREWARD-DATASET, we build a benchmark comprising 365 preference pairs for reward model evaluation. Each preference pair contains a *perfect* image, generated by a perfect

prompt, and a *perturbed* image generated from the corresponding perturbed prompt. Each preference pair undergoes rigorous human review and verification to ensure the reliability and consistency of the annotations. We evaluate a wide range of leading models on this benchmark using overall preference accuracy as the evaluation metric. The evaluation includes proprietary models such as GPT-5 [32] and Gemini-2.5 Pro [7], advanced open-source VLMs from the Qwen2.5-VL series [3] from 7B to 72B, as well as several existing image reward models: PickScore [17], ImageReward [53], UnifiedReward [49], and the HPS family [29, 52]. For UnifiedReward, we adopt its Qwen2.5-VL-based variants due to their superior performance. For the evaluation of proprietary models and the Qwen2.5-VL series, we instruct the VLMs to choose between the two images in each preference pair by selecting either 'the first image' or 'the second image'. Considering that model predictions may be sensitive to the presentation order of the images, we mitigate this potential bias by performing the evaluation twice, each time with the image order reversed. We then compute average accuracy across two evaluations to obtain a more robust and reliable performance metric.

### 8.3. Applying SpatialScore for Online RL

To further validate the improved spatial understanding through SPATIALSCORE, we use our reward model for online RL training. Specifically, the reward model is applied to RL fine-tuning the base model, Flux.1-dev [18], which supports the long-text prompts necessary to align with our complex spatial scenarios. Following the Flow-GRPO [25], we adopt LoRA-based RL fine-tuning and leverage the *perfect* prompts from our curated SPATIALREWARD-DATASET for GRPO training, employing the following hyperparameters: a LoRA rank of 32, a learning rate of  $3 \times 10^{-4}$ , an importance clipping range of  $1 \times 10^{-4}$ , a sampling group size of 24, and a KL-penalty coefficient of 0.01. The entire online RL training process is conducted on 32 NVIDIA H20 GPUs.

### 8.4. Evaluations for Image Generation

For evaluating the spatial understanding of image generation models, we first employ our proposed reward model SPATIALSCORE to assess in-domain performance in complex spatial reasoning using the prompts from our reward model evaluation benchmark. Beyond in-domain evaluation, we further adopt several out-of-domain benchmarks designed to measure text-image alignment, from which we specifically select the spatial-aware sub-dimensions to robustly evaluate spatial understanding in image generation.

### Instruction Template

You are tasked with evaluating a generated image based on Spatial Position Consistency. Please provide a rating from 0 to 10, with 0 being the worst and 10 being the best.

#### Spatial Position Consistency:

Evaluate how well the spatial relationships in the image match the descriptions in the prompt. Focus on the relative positions and arrangements of multiple objects in relation to each other and the background in the image. The following sub-dimensions should be considered:

- **Relative Positioning between objects.** Evaluate if the relative positions between the objects in the image match the description in the prompt. The objects should be placed in the described order and relative positions, without contradictions.
- **Relative Positioning with Background.** Evaluate if the relative positions of all objects with respect to the background in the image match the description in the prompt.
- **Consistency in Object Attributes.** Check if the properties of objects (such as size and color) at their specified positions align with the descriptions in the prompt. Ensure that the attributes of the objects are consistent with their spatial relationships.

Textual prompt: [text prompt]

Please provide the overall ratings of this image: <|Reward|>

END

In particular, we utilize DPG-Bench [14], which focuses on complex text-to-image alignment; TIIF-Bench [50], an extension of T2I-Compbench++ [47] to long prompts, evaluated by the proprietary model GPT-4o [1]; and the recently released UniGenBench++ [47], which is assessed by the powerful leading model Gemini-2.5 Pro [7]. and provides reliable multi-dimensional alignment evaluation.

## 9. Dataset Construction

### 9.1. Preference Pair Construction

For our curated SPATIALREWARD-DATASET, we construct 80k adversarial preference pairs for subsequent reward model training. To minimize the influence of other factors, such as aesthetic differences across image generation models, we generate each preference pair using a single image generation model while varying only the prompts. Specifically, we first employ GPT-5 [32] to create an initial set of prompts featuring complex spatial relationships among multiple objects. We then use GPT-5 to perturb these clean prompts by modifying one or more spatial relations (e.g., moving an object from left to right, swapping the relative positions of objects) while keeping the remaining relationships unchanged. Under this setup, images generated from the original, unperturbed prompts serve as the *perfect* images, whereas those generated from the perturbed prompts act as the *perturbed* images, thereby forming a complete preference pair. As illustrated in Figure 9 and Figure 10, we show several representative examples of preference pairs to visualize our curated SpatialReward-Dataset.

To further enhance the diversity of our dataset, we

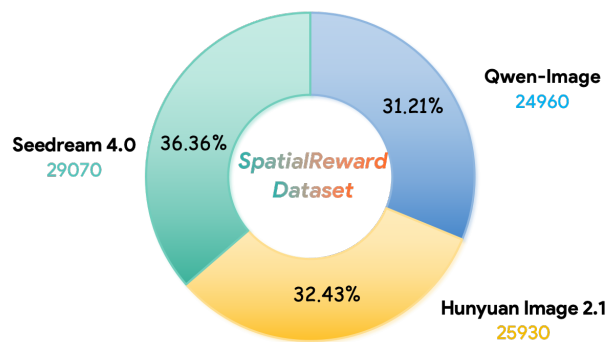


Figure 8. Distribution statistics of SpatialReward-Dataset.

employ several state-of-the-art image generation models Qwen-Image[51], HunyuanImage-2.1 [45], and Seedream 4.0 [8], which demonstrating strong text-image alignment capabilities, thereby mitigating the need for extensive manual filtering during subsequent human evaluation. For the generation of each preference pair, we randomly select one of the three models to produce both the *perfect* image and its corresponding *perturbed* image, ensuring that each pair is generated consistently by the same model. As illustrated in Figure 8, we present the distribution and proportions of preference pairs contributed by each model within our SpatialReward-Dataset.

### 9.2. Human Verifications

After collecting the initial preference prompts and generating the corresponding preference pairs, we perform an ad-

Perfect Text Prompts and Generated Images			Perturbed Text Prompts and Generated Images
<p>In a kitchen, a stovetop has two front burners. <b>A frying pan sits on the left burner, and a kettle sits on the right burner.</b> A pot lid leans against the backsplash behind the kettle. On the counter, a wooden spoon rests to the right of the stove, and a salt jar sits to the left of the stove.</p>			<p>In a kitchen, a stovetop has two front burners. <b>A kettle sits on the left burner, and a frying pan sits on the right burner.</b> A pot lid leans against the backsplash behind the kettle. On the counter, a wooden spoon rests to the right of the stove, and a salt jar sits to the left of the stove.</p>
<p>In a warehouse aisle, a stack of pallets is centered. <b>A forklift is parked in front of the pallet stack.</b> A warning cone stands to the right of the forklift, and a ladder leans to the left of the pallet stack. A safety sign hangs above the pallet stack.</p>			<p>In a warehouse aisle, a stack of pallets is centered. <b>A forklift is parked to the left of the pallet stack.</b> A warning cone stands to the right of the forklift, and a ladder leans to the left of the pallet stack. A safety sign hangs above the pallet stack.</p>
<p>At an outdoor market, a crate of apples sits on a wooden pallet. A chalk sign is placed in front of the crate. <b>To the right of the crate, a box of grapes is stacked, and to the left of the crate, a basket of pears is displayed.</b> A hand scale hangs above the center of the crate.</p>			<p>At an outdoor market, a crate of apples sits on a wooden pallet. A chalk sign is placed in front of the crate. <b>To the right of the crate, a basket of pears is displayed, and to the left of the crate, a box of grapes is stacked.</b> A hand scale hangs above the center of the crate.</p>
<p>In a home office, a desk is centered with a laptop in the middle. <b>A mouse sits to the left of the laptop, and a notepad sits to the right.</b> A chair is positioned in front of the desk, and a printer is placed behind the desk aligned with the left edge of the desktop.</p>			<p>In a home office, a desk is centered with a laptop in the middle. <b>A mouse sits to the right of the laptop, and a notepad sits to the left.</b> A chair is positioned in front of the desk, and a printer is placed behind the desk aligned with the left edge of the desktop.</p>
<p>On a study shelf, three framed photos stand in a row. <b>The photo of a lake is on the left, the photo of a mountain is in the center, and the photo of a dog is on the right.</b> A small clock is placed in front of the center frame aligned with its lower edge. A candle stands behind the lake photo. A bookmark leans against the lake photo's frame.</p>			<p>On a study shelf, three framed photos stand in a row. <b>The photo of a dog is on the left, the photo of a mountain is in the center, and the photo of a lake is on the right.</b> A small clock is placed in front of the center frame aligned with its lower edge. A candle stands behind the lake photo. A bookmark leans against the dog photo's frame.</p>
<p>In a bright kitchen, a wooden island holds a cutting board at the center. Sliced tomatoes lie on the left side of the board, and chopped onions lie on the right side. <b>A chef's knife rests at the board's back edge, and a mixing bowl sits behind the board.</b></p>			<p>In a bright kitchen, a wooden island holds a cutting board at the center. Sliced tomatoes lie on the left side of the board, and chopped onions lie on the right side. <b>A chef's knife rests at the board's front edge, and a mixing bowl sits behind the board.</b></p>
<p>In a city park, a wooden bench is centered with a large tree behind it, aligned with the bench's midpoint. On the bench seat, a folded newspaper lies between two items, <b>a stainless steel water bottle positioned at the left end and a backpack positioned at the right end.</b> A pigeon stands on the ground in front of the bench, aligned with the newspaper. A trash bin is placed to the left of the bench, aligned with its left armrest.</p>			<p>In a city park, a wooden bench is centered with a large tree behind it, aligned with the bench's midpoint. On the bench seat, a folded newspaper lies between two items, <b>a backpack positioned at the left end and a stainless steel water bottle positioned at the right end.</b> A pigeon stands on the ground in front of the bench, aligned with the newspaper. A trash bin is placed to the right of the bench, aligned with its right armrest.</p>
<p>In a dining room, a rectangular table is centered under a pendant light. A deep soup bowl sits at the center of the table, with a spoon placed to the left of the bowl and a fork placed to the right. A clear glass stands behind the bowl, aligned with its midpoint. <b>A folded napkin is positioned at the upper-left corner of the tabletop.</b> A candleholder is placed behind the glass, aligned with the bowl.</p>			<p>In a dining room, a rectangular table is centered under a pendant light. A deep soup bowl sits at the center of the table, with a fork placed to the left of the bowl and a spoon placed to the right. A clear glass stands behind the bowl, aligned with its midpoint. <b>A folded napkin is positioned at the upper-right corner of the tabletop.</b> A candleholder is placed behind the glass, aligned with the bowl.</p>
<p>On a rooftop garden, a rectangular planter is centered with a trellis rising behind it, aligned with the planter's midpoint. Two lanterns sit on the ground, one to the left of the planter and one to the right. A metal watering can is positioned behind the planter, slightly to the right. A cushion lies in front of the planter, aligned with the trellis. <b>The left lantern is bronze and the right lantern is blue.</b></p>			<p>On a rooftop garden, a rectangular planter is centered with a trellis rising behind it, aligned with the planter's midpoint. Two lanterns sit on the ground, one to the left of the planter and one to the right. A metal watering can is positioned behind the planter, slightly to the right. A cushion lies in front of the planter, aligned with the trellis. <b>The left lantern is blue and the right lantern is bronze.</b></p>
<p>In a stadium row, three seats labeled A, B, and C are arranged from left to right. <b>A popcorn bucket sits on seat A. A soda cup rests on seat B.</b> A program booklet lies on seat C. An aisle runs in front of the row, and a railing stands behind the row, centered with seat B.</p>			<p>In a stadium row, three seats labeled A, B, and C are arranged from left to right. <b>A popcorn bucket sits on seat B. A soda cup rests on seat A.</b> A program booklet lies on seat C. An aisle runs in front of the row, and a railing stands behind the row, centered with seat B.</p>

Figure 9. Visualization of the preference pairs (perfect images and perturbed images) in our SpatialReward-Dataset.



Figure 10. More visualizations of the preference pairs (perfect images and perturbed images) in our SpatialReward-Dataset.

ditional round of human verification to ensure the reliability and overall quality of our SPATIALREWARD-DATASET. Specifically, the verification follows two main principles:

1. Verification of perfect images. We examine whether each *perfect* image faithfully satisfies the complex spatial relationships across all objects in the prompt. If a perfect image contains clear violations of the specified spatial relations, the entire preference pair is discarded.
2. Verification of perturbed images. We assess the spatial discrepancies between the *perturbed* image and its corresponding *perfect* image. In some cases, although the perturbed prompt differs from the original prompt, the resulting spatial relationships may remain nearly identical. If the perturbed image fails to exhibit the intended spatial deviation and instead shares the same spatial layout as the perfect image, the preference pair is removed.

## 10. Additional Experiment Results

### 10.1. Applying SpatialScore to Qwen-Image

To further assess the effectiveness and robustness of our reward model SPATIALSCORE, we perform RL fine-tuning on advanced image generation models Qwen-Image [51]. As shown in Table 7, we observe consistent and significant improvements in spatial understanding compared to the base model Qwen-Image, similar to the comparisons on the Flux.1-dev [18]. On the in-domain SPATIALSCORE evaluation, our method improves from 6.74 to 8.25, demonstrating the effectiveness of RL training using SPATIALSCORE as the reward model. For other text-image alignment benchmarks, we select the spatial-aware sub-dimensions to assess spatial understanding, as discussed in the paper. As seen in Table 7, our RL training yields consistent improvements across both short-prompt and long-prompt settings.

### 10.2. Evaluations on Geneval Benchmark

Despite the fact that Geneval as a reward model, often yields unreliable evaluations under visual challenges such as occlusion and exhibits limited generalization to long

Table 5. Quantitative evaluations on the Geneval benchmark. Our model is trained using SpatialScore as the reward model.

Methods	Single object	Two object	Counting	Colors	Position	Color Attribute	Overall
Flux.1-dev	0.99	0.81	0.70	0.76	0.19	0.45	0.65
Ours	1.00	0.92	0.88	0.79	0.37	0.66	0.78

Table 6. Ablation study of SpatialScore backbone sizes on the reward evaluation benchmark. “1 Pert.” and “2–3 Pert.” denote subsets constructed by applying one or two–three spatial perturbations, respectively, to perfect prompts for perturbed prompts.

Setting\backbone	Qwen2.5-VL-3B	Qwen2.5-VL-7B	Qwen2.5-VL-32B
1 Pert.	0.861	0.939	0.955
2–3 Pert.	0.919	0.978	0.989
Overall	0.891	0.958	0.973

texts involving complex inter-object spatial relationships after RL training, we nonetheless utilize the Geneval benchmark to comprehensively assess the generalization of our model. Specifically, we conduct evaluations on the Geneval benchmark constructed by simple, fixed-template compositions. As shown in Table 5, our model, which employs SpatialScore-guided RL training, achieved significant zero-shot improvements across all evaluated metrics.

### 10.3. Ablations on Model Size

To investigate the generalization of our method, we train models with varying backbone sizes from the Qwen2.5-VL series [3]. As depicted in Table 6, the accuracy of pairwise preference prediction on our reward evaluation benchmark progressively increased from 0.891 to 0.958 and 0.973 as the backbone size scaled from 3B to 7B and 32B, respectively. Furthermore, by referencing the comparisons in the paper, we observe that the performance of SpatialScore with 7B size exceeds that of Gemini 2.5 Pro [7] and approaches the performance of the 32B variant. Consequently, considering the training efficiency for RL training, we finally select the 7B size configuration for all experiments.

Table 7. Detailed comparisons for the Qwen-Image family on SpatialScore, DPG-Bench, TIIF-Bench (short/long), and UnigenBench++ (short/long). \* denotes RL-training with our SpatialScore as the reward model. BR, AR, and RR denote basic relation, attribute+relation, and relation+reasoning. Lay-2D/3D refer to layout-2D/3D. Unibench denotes UnigenBench++.

Method	SpatialScore	DPG-bench	TIIF-bench-short			TIIF-bench-long			Unibench(short)		Unibench(long)	
		Relation-Spatial	BR	AR	RR	BR	AR	RR	Lay-2D	Lay-3D	Lay-2D	Lay-3D
Qwen-Image [51]	6.74	0.920	0.865	0.756	0.704	0.827	0.751	0.716	0.864	0.852	0.912	0.860
Ours*	<b>8.25</b>	<b>0.958</b>	<b>0.899</b>	<b>0.792</b>	<b>0.791</b>	<b>0.871</b>	<b>0.801</b>	<b>0.780</b>	<b>0.908</b>	<b>0.917</b>	<b>0.926</b>	<b>0.893</b>

#### 10.4. Understanding of Spatial Issues in T2I models

The core issue is the misalignment between training captions and complex inference prompts. Current T2I models are trained on MLLM-derived captions, which mainly describe the existence of multiple objects but lack complex constraints of spatial relationships between them. Thus, these models are prone to spatial errors for long, spatially complex prompts. Moreover, existing reward models mainly focus on aesthetics and semantic alignment, and Figure 1 in our paper shows these models fail to correctly penalize spatial errors. We propose the first reward model designed for spatial understanding.

#### 10.5. More Clarifications on NFE

In the paper, we present comparisons on the number of function evaluations (NFEs) [28] for ablations of Top- $k$  filtering. Here, we provide a detailed explanation of its calculation. Specifically, NFE refers to the number of forward passes of the policy model exclusively for the computation of the policy ratio  $r(\theta)$  during the training stage, and not the sampling stage. Given a sampling group size of 24 per prompt and 6 denoising steps, the NFEs differ based on the setup. For the original GRPO setup without top- $k$  filtering, the requirement is  $24 \times 6$  NFEs per prompt at each training step for the training stage. For our GRPO setup adding top- $k$  filtering, we select a total of  $2 \times k$  samples (comprising top- $k$  and bottom- $k$ ) after the sampling stage. We then use these filtered samples for the training stage, consequently requiring  $2 \times k \times 6$  NFEs per prompt at each training step.

#### 10.6. More Visual Demos

As shown in Figure 11, we provide more qualitative comparisons between the base model Flux.1-dev [18] and the Flux variant trained with Flow-GRPO on the Geneval. Our RL-trained model with SPATIALSCORE demonstrates improved spatial understanding, generating images that more accurately reflect the complex spatial relationships between multiple objects as described in the prompts. In contrast, the Flux.1-dev variant, trained with Flow-GRPO on Geneval, exhibits limited generalization for complex spatial relationships, even losing part of the base model’s ability to follow long prompts. As shown in Figure 11, this includes missing key objects, such as the candles in Example (1) and the

soap and toothbrush in Example (2). Furthermore, due to its reliance on rule-based rewards from object detectors, the Flux variant guided by the Geneval frequently generates images with visually implausible artifacts, such as the napkin floating in mid-air, as seen in Example (5).

### 11. Limitations and Future Works

Although we have validated the enhancement of spatial understanding through reward modeling at the image level, the integration of spatial understanding with temporal dynamics has not been fully explored, particularly with regard to video generation. Video generation requires models to not only comprehend static spatial relationships but also to account for dynamic changes over time. For instance, a model may need to move object A to the left of object B, then place object C to the right of object B, and subsequently swap the positions of objects A and C. Therefore, an essential challenge for future work will be to effectively extend reward modeling to enhance the spatial understanding of video generation models. This direction is especially important for sim-to-real embodied simulation scenarios, where generating temporally consistent and spatially accurate video sequences is critical for bridging the gap between simulated environments and real-world dynamics.

### Text Prompt with complex relations

1

In a dining room, a sideboard holds a large platter **centered** under a framed painting. Two candlesticks flank the platter, a tall candlestick to the **left** and a short candlestick to the **right**. A bowl of grapes sits **behind** the platter, aligned with its midpoint. A loaf of bread rests in **front** of the platter, **centered**. A folded runner lies along the sideboard's **top edge**.

2

In a bathroom, a sink cabinet is **centered** under a mirror. A soap dispenser stands to the **left** of the faucet, and a toothbrush holder stands to the **right** of the faucet. A towel rack is mounted to the **right** of the mirror. A bath mat lies in **front** of the sink, and a laundry basket sits to the **left** of the cabinet.

3

In a hallway table display, a bowl of keys sits to the **left**. A vase sits to the **right**. A photo frame stands **behind** the bowl. A small sculpture stands **behind** the vase. A runner lies **centered** under all items. A lamp is placed between the bowl and the vase **centered**.

4

In a parking lot, a red car is **centered**. A blue car is parked **behind** the red car slightly to its **left**. A shopping cart stands in **front** of the red car toward its **right** side. A lamppost stands to the **left** of the blue car, and a sign stands to the **right** of the shopping cart.

5

On a breakfast tray, a bowl of cereal sits at the **center**. A spoon rests to the **right** of the bowl aligned with its rim. A glass of orange juice stands to the **left** of the bowl aligned with its rim. A sliced banana lies in **front** of the bowl, with the slices **forming a row**. A napkin is folded **behind** the bowl **centered**.

Flux

Flow-GRPO  
(GenEval)

Ours



Figure 11. More qualitative comparisons of the long prompts with complex spatial relationships across objects.